Quantitative flow visualization of a turboprop aircraft by robotic volumetric velocimetry

Sciacchitano, Andrea; Giaquinta, Daniele; Schneiders, Jan; Scarano, F.; van Rooijen, B.D.; Funes, D.E.

DOI
10.3929/ethz-b-000279206

Publication date
2018

Document Version
Final published version

Published in
Proceedings 18th International Symposium on Flow Visualization

QUANTITATIVE FLOW VISUALIZATION OF A TURBOPROP AIRCRAFT BY ROBOTIC VOLUMETRIC VELOCIMETRY

A. Sciacchitano[1,c], D. Giaquinta[1], J.F.G. Schneiders[1], F. Scarano[1], B.D. van Rooijen[2], D.E. Funes[3]

[1]Department of Aerospace Engineering, Delft University of Technology, Delft, The Netherlands
[2]German-Dutch Wind Tunnels DNW, Marknesse, The Netherlands
[3]Airbus Military, Getafe, Spain
[c]Corresponding author: Tel.: +31152788692; Email: a.sciacchitano@tudelft.nl

KEYWORDS:
Main subjects: Quantitative flow visualization, turboprop aircraft
Fluid: Incompressible flow, tip vortices, propellers
Visualization method(s): Robotic Volumetric Velocimetry
Other keywords: Large-scale Particle Image Velocimetry, helium-filled soap bubbles

ABSTRACT: *The flow field around a turboprop aircraft scaled model is investigated with attention to the propeller slipstream and the wing near wake. The experiments are conducted in the Low-Speed Tunnel (LST) of the German-Dutch Wind Tunnels (DNW) as part of a collaboration among DNW, Delft University of Technology and Airbus. Quantitative flow visualization in a three-dimensional measurement domain of 150 liters is made possible by the use of the recently developed Robotic Volumetric Velocimetry technique. Time averaged velocity and vorticity fields are obtained for experiments carried out at 8 m/s and 50 m/s, respectively. The measurements are conducted with high-speed acquisition in multi-frame mode at 8 m/s, and require double-frame mode at 50 m/s. The presence of three coherent streamwise vortices is revealed, emanating from the wing tip, the flap side edge and the engine nacelle, respectively. A comparison between the two measurement conditions shows limited Reynolds number effects on the wing tip vortex, and that the multi-frame measurements are superior in terms of spatial resolution and measurement accuracy.*

1 Introduction

The three-dimensional flow around turboprop aircraft exhibits complex features as it entails propeller slipstream and the wing flow interactions. The aerodynamic design verification of such aircraft relies upon a combination of numerical simulations, wind tunnel measurements and flight tests. The latter two are typically conducted to validate the accuracy of CFD simulations. In wind tunnel testing, integral aerodynamic loads and the loads distribution on aircraft are determined via force balance measurements and surface pressure measurements. In addition, flow visualization techniques such as surface oil flow visualization are sometimes employed to study finer details of the flow field topology [1]. Since its introduction, Particle Image Velocimetry (PIV) has proven its value to enable the quantitative visualization of velocity and vorticity of the flow structures around aircraft. Pengel et al. [2] demonstrated the feasibility of using planar PIV in the large low-speed wind tunnel (LLF) of the German-Dutch Wind tunnels (DNW) to investigate the wake vortices of a twin-engined Airbus model. Roosenboom et al. [3] used two-component PIV to investigate the slipstream of an 8-bladed propeller. The measurements revealed secondary boundary layer vortices formed in the slipstream that move with the wake blade and cause periodic flow separation. Various applications of PIV in aeronautics are reported that characterize the aerodynamics of high-lift configurations, wake vortices, propeller and rotor flows [4]. For example, Arnott et al. [5] employed planar PIV in the industrial low-speed wind tunnel of Airbus Bremen (Germany) to study the flow field of a wing model equipped with slat and

flap in high-lift configuration. Veldhuis et al. [6] demonstrated the applicability of PIV diagnostics for wake vortex research in towing tank facilities, by conducting measurements over a 1:48 Airbus A340-300 scaled model. More recently, Sinnige et al. [7] made use of stereoscopic PIV in the Low-Speed Facility of DNW to investigate the effect of pylon trailing edge blowing on the interaction between pusher propeller and its associated pylon wake.

Despite its advancements, the application of PIV in aeronautics poses several technical challenges as a result of its working principle and some physical limitations. Measurements are often limited to small regions to characterize local effects as announced by preliminary CFD analysis. A more holistic approach yielding the full three-dimensional flow structure around an aircraft has never been attempted so far, although it may arguably serve as more extended and versatile source of information for validating numerical simulations.

The introduction of helium-filled soap bubbles (HFSB) as flow tracers has greatly increased the measurement domain of PIV experiments, making large-scale PIV possible [8]. Their use in aerodynamic wind tunnel flows is recent [9]. Aerodynamic applications to vortex dominated flows have indicated the suitability of HFSB to produce an accurate estimate of the flow velocity in the low-speed regimes [10, 11]. Large-scale tomographic PIV experiments could be conducted that investigate the tip vortex of a vertical axis wind turbine blade over a measurement volume exceeding 12 liters. The recent introduction of the coaxial volumetric velocimetry (CVV, [12]) has simplified significantly the operations needed to setup a tomographic system (cameras field-of-view setting, illumination, system calibration). Moreover the CVV technique enables three-dimensional PIV measurements around objects of complex shape where the optical access is limited to only one direction. Due to the compactness of the CVV optical head, its handling via a robotic arm showed to be a viable solution yielding a versatile approach to three-dimensional measurements, which has achieved measurement volumes of the order of the cubic meter (robotic volumetric velocimetry, RVV, [13]). Using RVV, Jux et al. [13] conducted flow measurements around a full-scale cyclist model at free-stream velocity of 15 m/s. The measurements around a model with significant geometrical complexity and large size demonstrated the potential of the technique for applications in industrial wind tunnels for aircraft aerodynamics investigation. The work of Jux et al. [13] coupled the measurement of HFSB images with the Lagrangian Particle Tracking approach Shake-the-Box developed by Schanz et al. [14]. As a result, time average measurements were based on particle trajectory estimation from multiple observations of the same particle (typically 5 to 13 images). Due to the limited framing rate of the CVV imaging hardware, experiments at higher flow velocity are not possible within the above approach and only two subsequent exposures can be taken at an arbitrary time separation, which is the technique followed in the present work.

RVV is used here to achieve the three-dimensional velocity and vorticity visualization around the scaled model of an Airbus C-295 transport aircraft. Flow measurements are conducted at free-stream velocities of 8 m/s with multi-frame Lagrangian Particle Tracking (i.e. Shake-the-Box). Experiments are extended to free stream velocity of 50 m/s, where the particle images are acquired in double-frame mode. An additional challenge is posed in the latter regime by the reduced seeding concentration.

2 Setup of the experiment

2.1 Wind tunnel and aircraft model

Experiments are conducted in the Low Speed Tunnel (LST) of the German-Dutch Wind Tunnels (DNW). The LST is a closed-loop closed-test-section wind tunnel which features a contraction ratio of 9:1, a test section of 3×2.25 m^2, and a maximum free-stream velocity of 80 m/s. The wind tunnel model is a 1:12 scaled version of the EADS CASA C-295 aircraft, a twin-turboprop tactical military transport aircraft. The model is 1.97 m long and has a wing span of 2.15 m with 0.21 m mean chord. The model is connected to the LST six-component external balance mounted on the ceiling of the test section. The measurements are conducted at free-stream velocity of 8 and 50 m/s, with the aircraft in the take-off configuration at 9 degrees angle of attack and the flaps deployed at 10 degrees. The aircraft propeller is set at a rotating speed of 1550 and 9600 rpm for the two velocity cases, respectively, corresponding to a tip advance ratio of 0.96. The geometrical parameters of the aircraft model are summarized in Table 1.

Table 1. Geometrical parameters of the wind tunnel model.

Aircraft model parameter	Parameter symbol	Value
Model length	L	1.97 m
Wing span	b	2.15 m
Mean chord	c	0.21 m
Angle of attack	α	9 deg
Flaps deflection angle	δ	10 deg
Propeller tip advance ratio	J	0.96

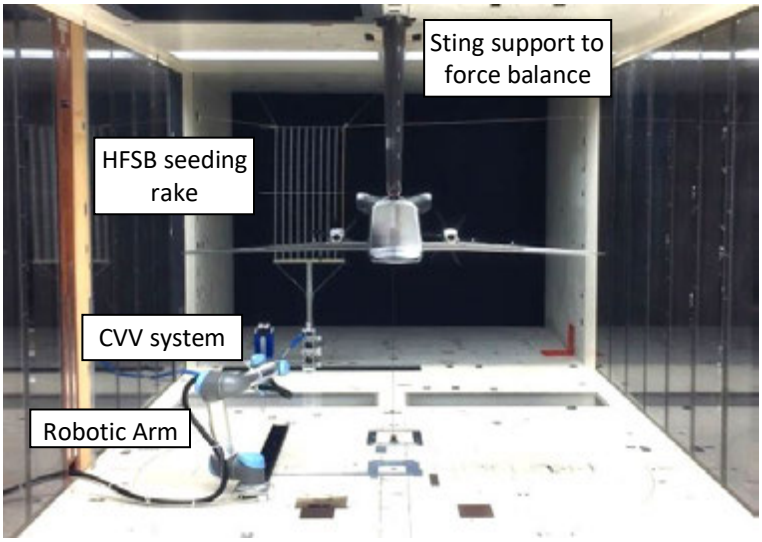

Fig. 1. Setup of wind tunnel model, HFSB seeder and robotic volumetric velocimetry system.

2.2 HFSB seeding system

The flow is seeded with helium-filled soap bubbles within a finite streamtube in the wind tunnel. The seeding system is placed at the end of the wind tunnel contraction and has a cross section of 1.0 (height) × 0.45 (width) m^2. The bubbles diameter ranges between 0.3 and 0.6 mm and the amount of helium and soap is controlled to obtain nearly neutral buoyancy. The seeder is visible in Fig. 1. It features 10 thin airfoils hosting 200 miniature bubble generators, releasing approximately 10^6 bubbles/s in the free stream. The resulting concentration of tracers depends upon the operating speed of the wind tunnel. In the present case, a relevant parameter is the concentration of detected tracers trajectories over the sequence of 9,000 image recordings. At 8 m/s the measurements yield approximately 10^2-10^3 tracks/cm^3. At 50 m/s the distribution appears less homogeneous and large portions of the domain feature a tracks concentration below 20 tracks/cm^3 (see Fig. 2).

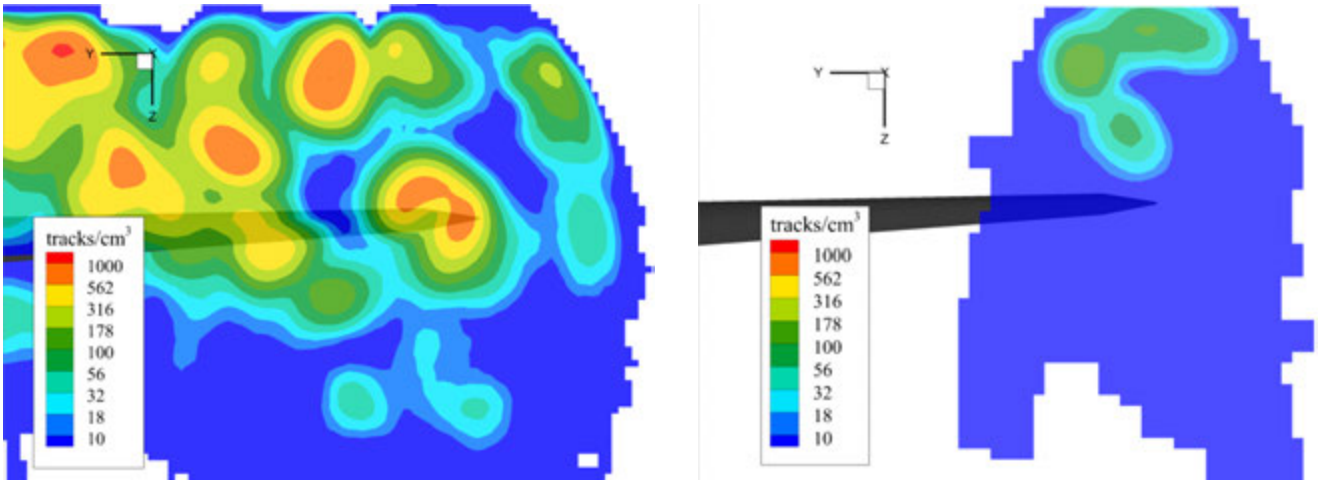

Fig. 2. Number of particle tracks per cubic centimeter at $x/c = 1$, being $x = 0$ the leading edge location at the wing root. Left: multi-frame measurements at $U_\infty = 8$ m/s; right: double-frame measurements at $U_\infty = 50$ m/s.

2.3 Robotic Volumetric Velocimeter

The RVV system is based on the three-dimensional manipulation of a Coaxial Volumetric Velocimeter (CVV, [12]). The latter comprises a four digital camera compact arrangement (CMOS, 10 bits, 832×632 pixels at 471 fps, 4.8 μm pixel pitch) with low tomographic aperture, to allow the detection of tracers in three-dimensional space. The illumination is provided by a Quantronix Darwin-Duo Nd:YLF laser (2×25 mJ pulse energy at 1 kHz, 527 nm wavelength). The light is transmitted via an optical fiber to the CVV head and from there it expands conically along the same axis as that formed with the region viewed by the four cameras (coaxial condition). The resulting measurement region features a truncated cone with about 20 cm in height and width, and 30 cm in depth. The CVV manipulation is performed with a UR5 collaborative arm that controls the motion and orientation of the CVV within a reach radius of 85 cm.

The measurements conducted at free-stream velocity U_∞=8 m/s are performed operating the CVV in continuous acquisition (*multi-frame mode*) at a rate of 471 images per second. Each run comprises a sequence of 9,000 images (19 seconds acquisition time). A typical number of 800 particles per image is retrieved, yielding a particle image density of 0.002 particles per pixel (ppp). The recordings are pre-

processed via a temporal high-pass filter [15] to increase the contrast between particle images and background reflections. A Gaussian smoothing in a 5×5 pixels kernel is applied thereafter. The motion of the particle tracers is extracted from the images using the Shake-the-Box algorithm [14]. A total of 15 measurement cones is required to capture the flow field in the wake of the wing and around the engine nacelle, resulting in a total measurement volume of approximately 150 liters (Fig. 3). The scattered instantaneous velocity data are averaged within cubic cells or *bins* of 30×30×30 mm^3 where the volume time-averaged velocity field is returned. Adjacent bins overlap by 75%, resulting in a Cartesian grid of velocity vectors with 7.5 mm pitch.

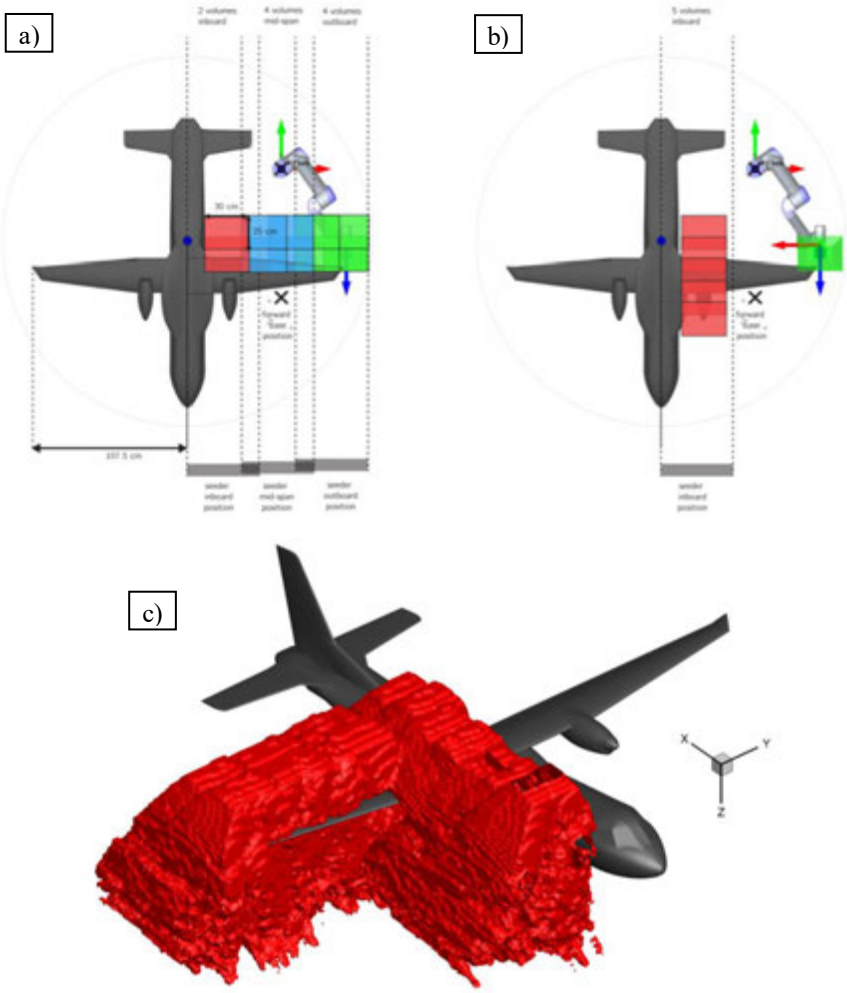

Fig. 3. Measurement cones for the multi-frame velocity measurements at U_∞ = 8 m/s. a) Wake flow measurements. b) Propeller flow measurements. c) Total measurement volume.

The experiments at U_∞ =50 m/s are only possible in frame-straddling mode (*double-frame measurements*). Due to the high flow velocity, a particle in the free-stream would move by over 10 cm between two successive recordings if recorded in multi-frame mode, which is deemed excessive to successfully track the particle tracers along their trajectories. Instead, image pairs are acquired using first a short time separation (65 µs) to produce a coarse estimation of the mean flow. A second set is acquired with a longer time separation (200 µs) that delivers a more accurate estimate of the particle

tracers displacement. Measurements are conducted only in the wake of the wing (10 measurement cones) and not in the engine nacelle region. Due to the higher free-stream velocity, the seeding concentration is strongly reduced with respect to the 8 m/s measurements [10], and the ppp decreases to about 0.0001. The three-dimensional particle distribution is reconstructed with the Iterative Particle Reconstruction algorithm [16], and their motion is tracked with an in-house Matlab algorithm. The statistical results are obtained by averaging the instantaneous velocity data in bins of 50×50×50 mm^3 volume with 75% overlap factor, resulting in a vector pitch of 12.5 mm.

3 Results

3.1 Multi-frame velocity measurements at U_∞ = 8 m/s

The analysis of the flow in the slipstream of the propeller is presented first. The propeller imparts an acceleration to the fluid along its axial direction. Immediately downstream of the propeller (x/c = –0.5, being x = 0 the leading edge location at the wing root, see Fig. 4-a), the streamwise velocity component reaches up to 130% of the free-stream value. The in-plane velocity vectors are consistent with the counter-clockwise rotation of the propeller. Past the leading edge locations (x/c = 0, Fig. 4-b), the streamwise velocity component further increases up to 150% of U_∞ over the suction side of the aircraft wing. Furthermore, a streamwise vortex is generated above the engine nacelle due to the interaction between the upward motion induced by the propeller at the inboard part of the wing and the downward motion on the suction side of the wing. According to the lifting line theory, such vortex is consistent with the increase of lift at the inboard part of the wing. At the wing trailing edge (Fig. 4-c), the streamwise acceleration induced by the propeller is still observed. The velocity vectors are mainly directed downwards due to the 9-degree angle of attack of the wing and the absence of flow separation on the suction side.

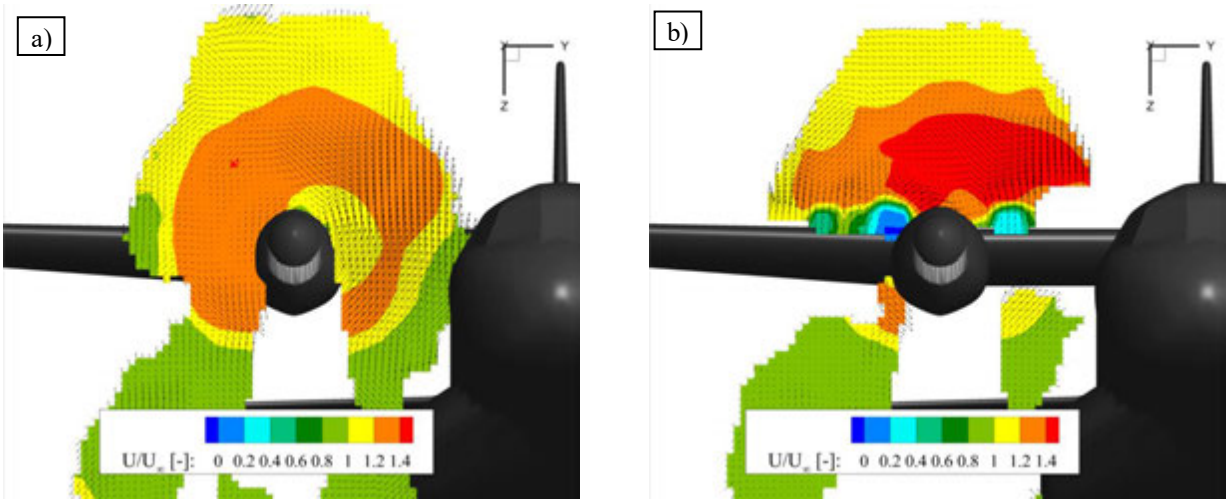

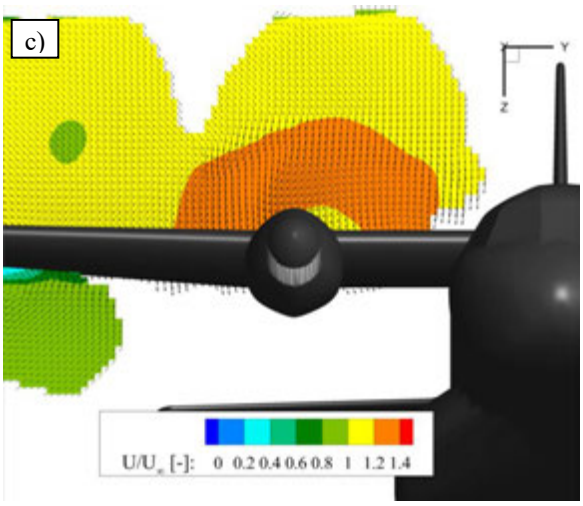

Fig. 4. Velocity field in the slipstream of the propeller for the multi-frame velocity measurements at U_∞ = 8 m/s. Contours of streamwise velocity components with in-plane velocity vectors. a) x/c = -0.5; b) x/c = 0; c) x/c = 1.

Fig. 5 shows the streamwise velocity component in a vertical plane located inboard with respect to the engine nacelle ($y/(b/2)$ = –0.22, being y = 0 the symmetry plane location). The flow accelerates on the suction side of the wing, reaching a maximum velocity of about 1.5 U_∞. Downstream of the wing trailing edge, lower streamwise velocity is retrieved due to the wing's wake. The out-of-plane velocity component causes streamlines crossing the examined data section, thus indicating that the flow is not two-dimensional.

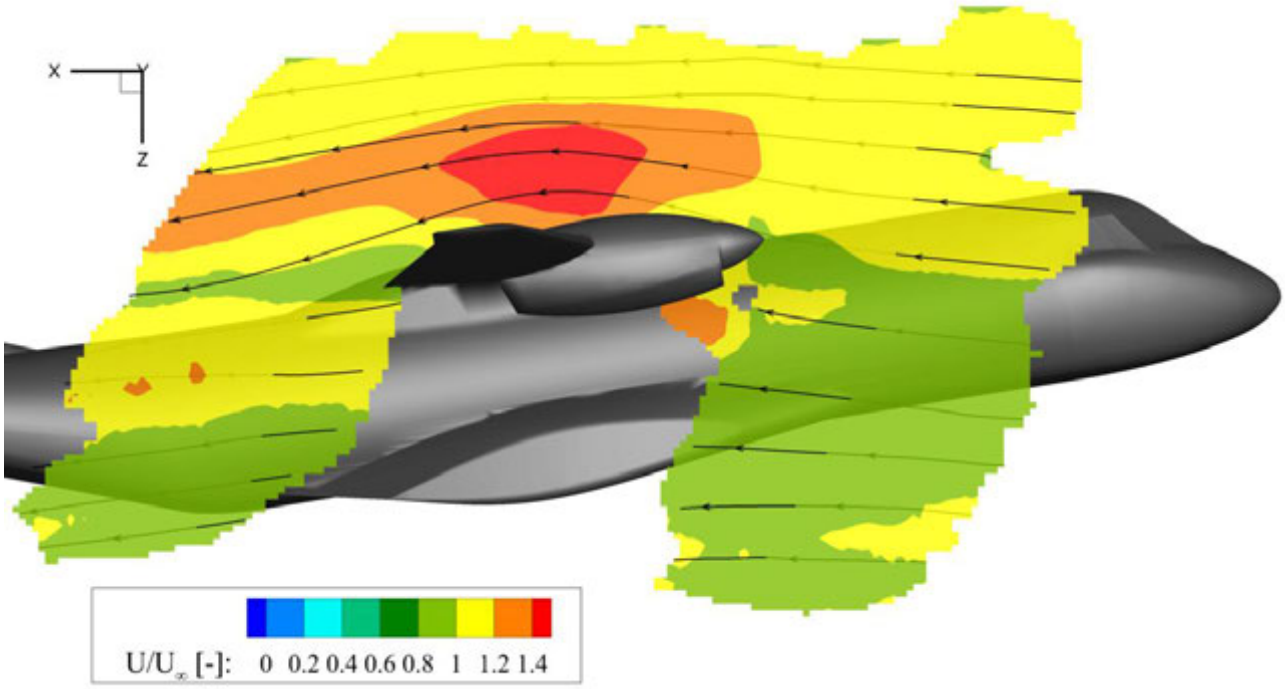

Fig. 5. Streamwise velocity field with streamlines at $y/(b/2)$ = -0.22.

The streamwise velocity and vorticity components in the wake of the wing at x/c = 1.8 are illustrated in Fig. 6. The velocity field of Fig. 6-top shows that the propeller-induced acceleration is still present in the wake of the wing, with the streamwise velocity component exceeding U_∞ by about 25%.

Furthermore, the flow has higher velocity than the free-stream on the suction side of the wing, whereas it has lower velocity on the pressure side, which is consistent with the generation of lift.
The vorticity field (Fig. 6-bottom) reveals the presence of three streamwise vortices. The first emanates from the wing tip, while a second one is produced by the flap edge at approximately 60% of the wing half-span. The two vortices are co-rotating, consistently with the lift discontinuity imposed at wing tip and flap edge. Additionally, another streamwise vortex, counter-rotating with respect to the previous ones, is detected on the inboard side of the engine nacelle and is ascribed to the interaction between the propeller-induced upwash and the downwash on the wing suction side. High stream-wise vorticity is also encountered at the tip of the propeller blades due to the shear layer generated by the propeller rotation.
An illustration of the three-dimensional vortical structures in the flow field is presented in Fig. 7, where three coherent streamwise vortices are retrieved, namely the wing tip vortex ($y/(b/2) = -1$), the flap side-edge vortex ($y/(b/2) = -0.6$) and the engine nacelle vortex ($y/(b/2) = -0.25$). The former two have a peak vorticity of 280 Hz and 180 Hz, respectively, and remain spatially coherent within the entire measurement volume (up to $x/c = 2.6$), whereas the engine nacelle vortex features lower intensity (peak vorticity of –100 Hz) and loses coherence at about $x/c = 2.2$.

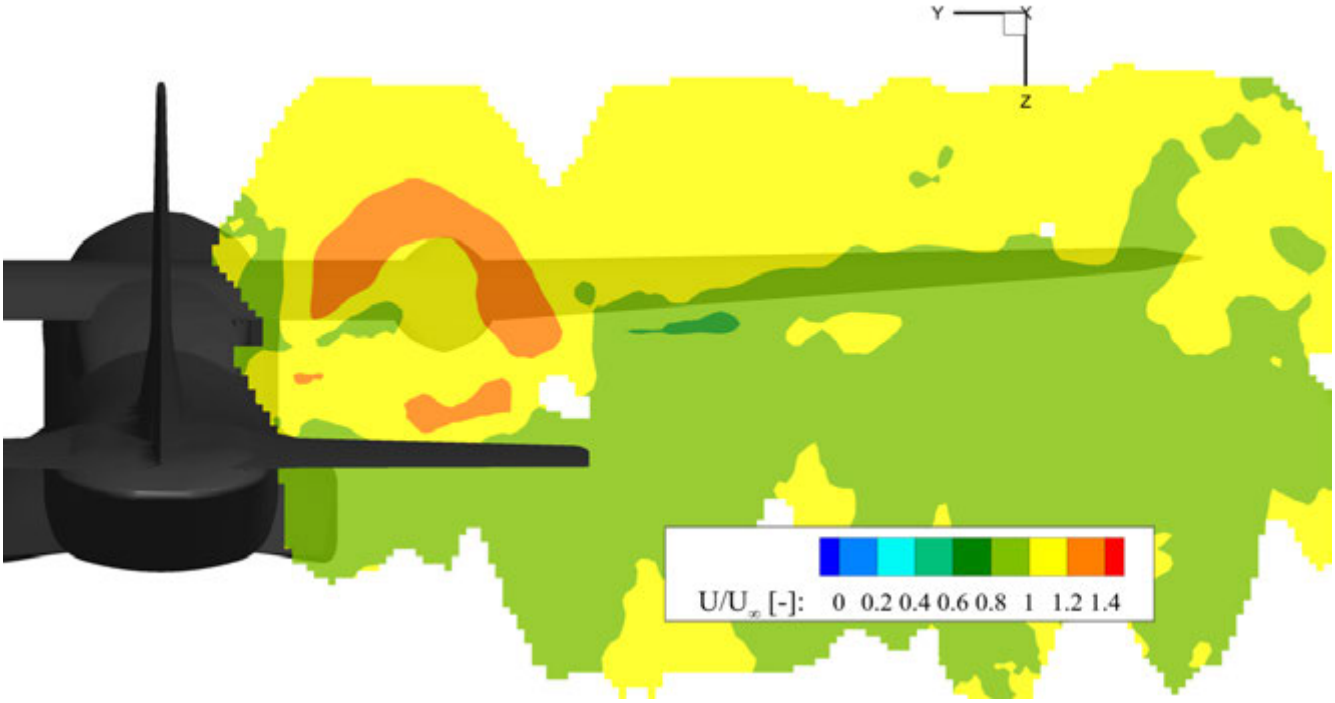

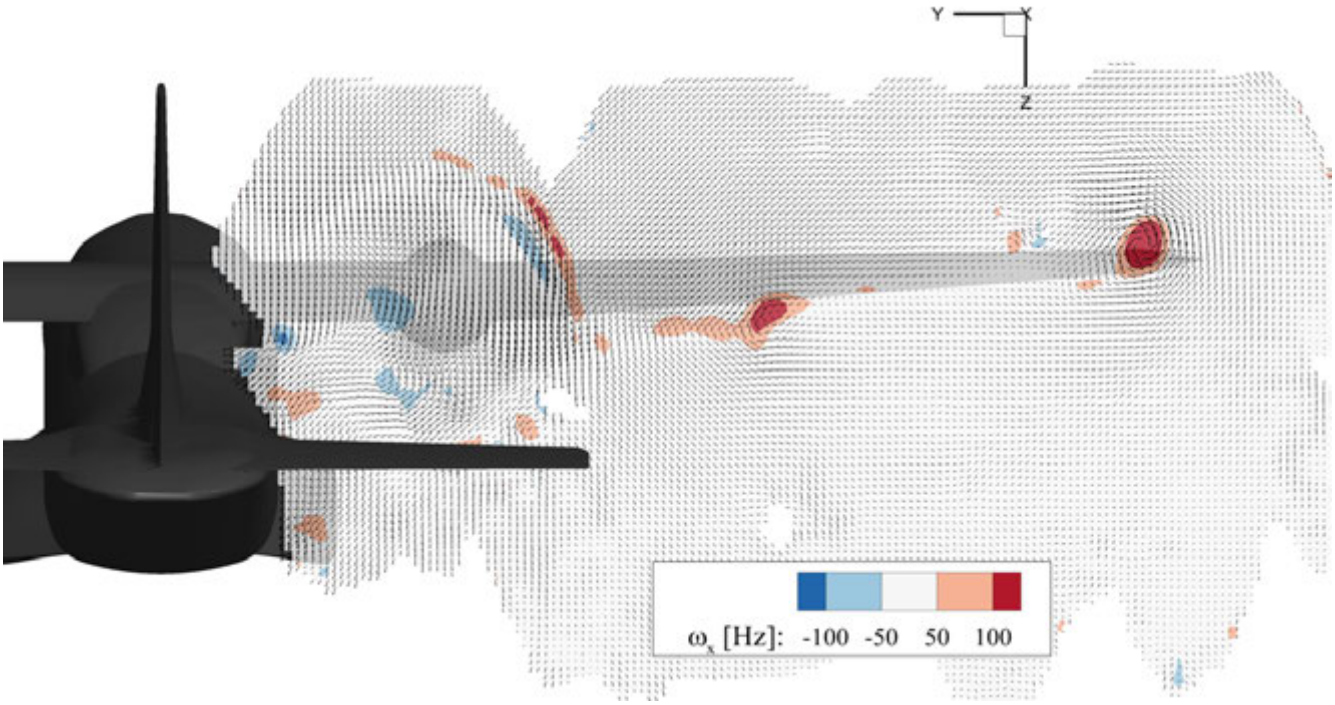

Fig. 6. Streamwise velocity field (top) and vorticity field with in-plane velocity vectors (bottom) in the wake of the wing at *x*/*c* = 1.8.

Fig. 7. Illustration of the vortical structures in the flow field. Iso-surfaces of Q-criterion (Q = 1000 s^{-2}) color-coded by streamwise vorticity.

3.2 Double-frame measurements at U_∞ = 50 m/s

The double-frame measurements in the wing tip region reveal the presence of a strong wing-tip vortex (Fig. 8). The peak vorticity (ω_{max} = 800 Hz) is significantly higher than in the multi-frame measurements due to the increased free-stream velocity. The vortex exhibits high spatial coherence throughout the entire measurement domain up to x/c = 2 (Fig. 9).

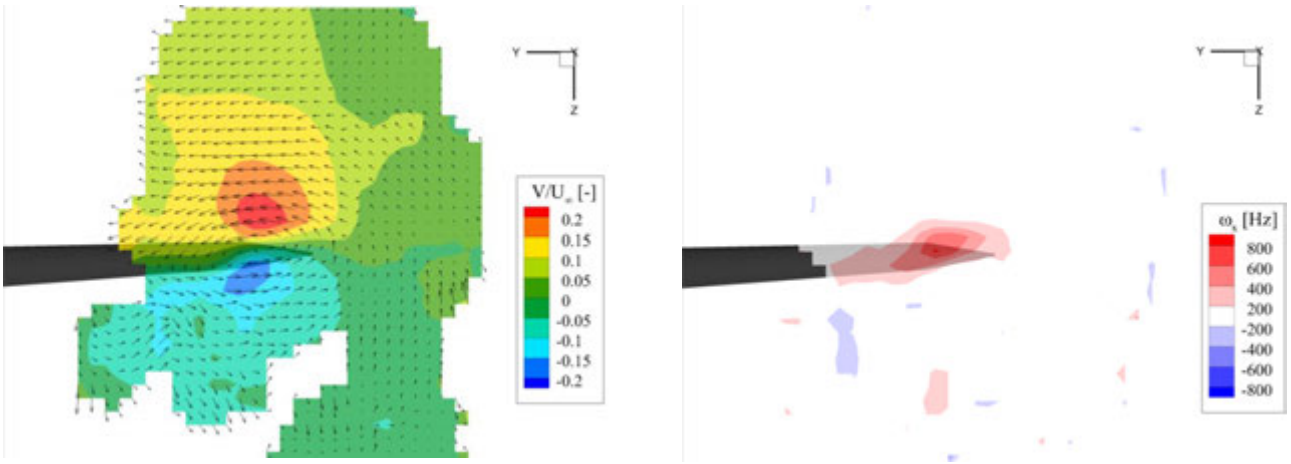

Fig. 8. Spanwise velocity component with in-plane velocity vectors (left) and streamwise vorticity component (right) at x/c = 1 for the double-frame measurements.

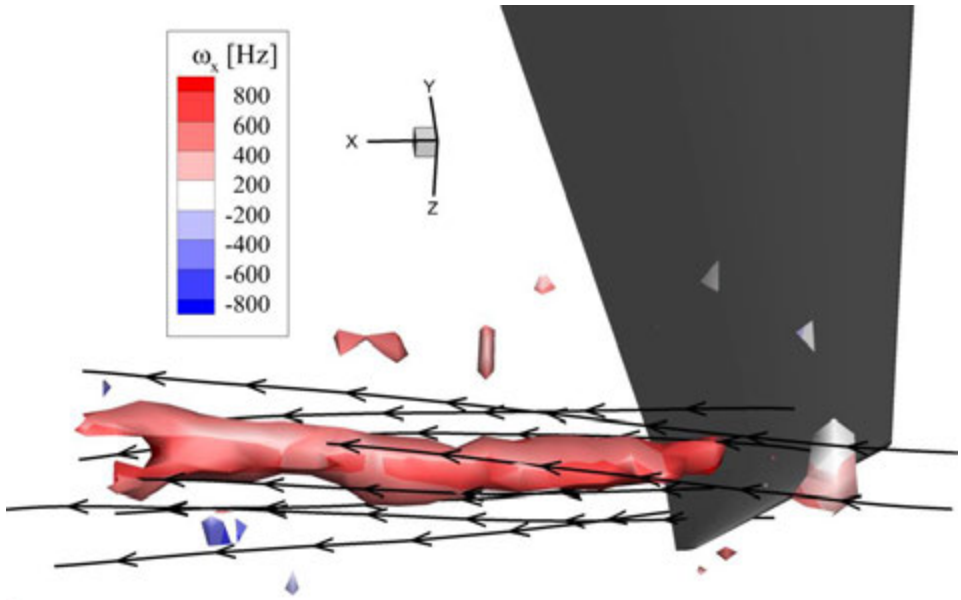

Fig. 9. Illustration of the wing tip vortex in the double-frame measurements. Iso-surfaces of Q-criterion (Q = 60000 s^{-2}) color-coded by streamwise vorticity.

3.3 Discussion of measurement uncertainties

As discussed by Caridi et al. [10], the seeding concentration in large-scale PIV experiments is inversely proportional to the flow velocity at the location where the tracer particles are released, which in this

case corresponds to the free-stream velocity U_∞. As a consequence, the double-frame measurements at U_∞ = 50 m/s feature a seeding concentration which is about six time lower than that of the multi-frame measurements at U_∞ = 8 m/s. As reported in section 2, to enhance the statistical convergence of the results, the statistical analysis for the double-frame data is conducted within larger bins (bin size of 50×50×50 mm^3 for the measurements at U_∞ = 50 m/s and 30×30×30 mm^3 for the measurements at U_∞ = 8 m/s). A comparison of the number of particle tracks concentration at x/c =1 was shown in Fig. 2. In the multi-frame measurements at U_∞ = 8 m/s, most interrogation bins contain more than 100 particles. In the wake of the wing, the number of particles per bin typically exceeds 1000, with peaks of above 10^4 in the wing tip region. Conversely, in the double-frame measurements at U_∞ = 50 m/s the number of particles per bin is significantly lower, with values of about 300 at the wing tip. Clearly, the reduced number of particles per bin of the double-frame data increases the uncertainty of the time-averaged velocity results.
Additional challenges associated with the double-frame measurements are the lower illumination intensity and the lower accuracy of the double-frame approach. Since the double-frame measurements require two separate laser pulses at a relatively short time separation, the illumination intensity (and therefore the amount of light scattered by the tracer particles) is reduced by about 50% with respect to the multi-frame measurements, where the two laser pulses shoot simultaneously. Furthermore, the multi-frame approach has been demonstrated to reduce the measurement uncertainty by factor $k^{3/2}$, being k the number of locations at which a tracer particle is tracked along its trajectory ([17].

Sections 3.1 and 3.2 have shown that a coherent wing tip vortex is visible both at U_∞ = 8 m/s and U_∞ = 50 m/s. A quantitative comparison of the vertical velocity and the vorticity magnitude of the vortex is illustrated in Fig. 10. The vertical velocity profile at U_∞ = 8 m/s reproduces a typical vortex profile, with an approximately constant velocity gradient in the vortex core and distinct minimum and maximum velocity values (Fig. 10-left). The core radius is about 25 mm and the peak velocity reaches 25% of the free-stream velocity. In the double-frame measurements at U_∞ = 50 m/s, the velocity peaks are still visible, although they assume lower value than in the low-speed measurements (W_{peak} = 0.1 U_∞). Due to the low number of tracer particles per interrogation bin, the measurement uncertainty is about 30% of the peak velocity measurements, significantly affecting the shape of the velocity profile.
The vorticity magnitude profile (Fig. 10-right) exhibits a clear peak located inboard with respect to the wing tip. The peak is higher for the multi-frame measurements at U_∞ = 8 m/s, with a non-dimensional vorticity value exceeding 6. The double-frame measurements at U_∞ = 50 m/s return a vorticity peak that is lower and broader than in the multi-frame measurements. The peak value reduction by about 50% is consistent with the lower spatial resolution of the double-frame measurements, caused by the choice of larger size of the statistical bins. Instead, the broader vorticity peak is attributed to the increased amplitude of meandering of the wing tip vortex due to the higher free-stream turbulence intensity [18].

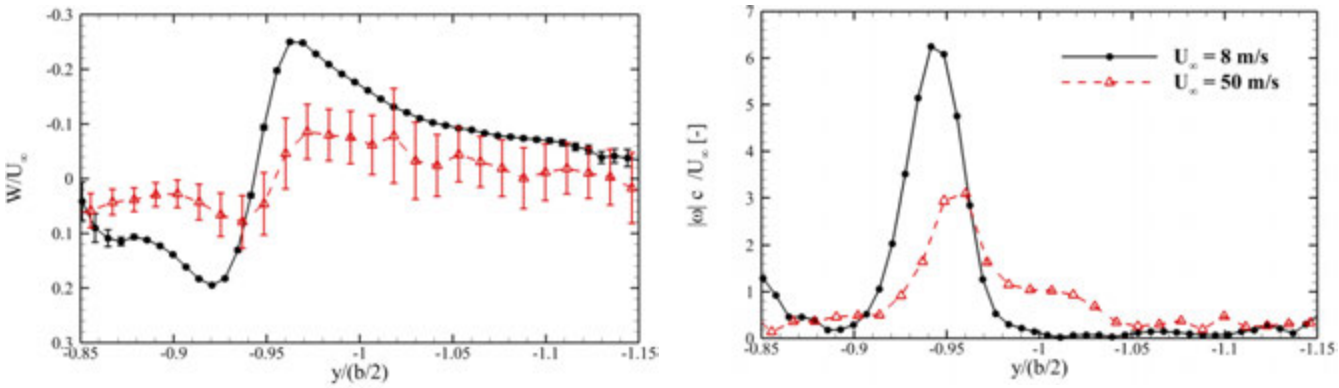

Fig. 10. Profiles of vertical velocity (left) and vorticity magnitude (right) at *x/c* = 1.5 at the height of the wing trailing edge. A positive W corresponds to a downward velocity component. The error bars on the mean velocity represent the measurement uncertainty at 95% confidence level. The symbol key applies to both plots.

4 Conclusions

Wind tunnel measurements have been conducted in the Low-Speed Tunnel (LST) of the German-Dutch Wind Tunnels (DNW) on a 1:12 scaled version of the EADS CASA C-295 aircraft. The three-dimensional flow field in the propeller slipstream and the wing near wake has been measured via the recently developed robotic volumetric velocimetry technique. The latter makes use of a compact velocimeter composed of four cameras at low tomographic aperture and a co-axial arrangement between imaging and illumination. A collaborative robotic arm is employed to move the velocimeter with millimeter precision, thus enabling a total measurement volume of 150 liters.

Flow measurements have been carried out at free-stream velocities of 8 m/s and 50 m/s in multi-frame mode and double-frame mode, respectively. In the first case, the position of tracer particles could be tracked over several successive time instants, thus retrieving Lagrangian particle tracks. In the double-frame measurements, instead, the tracer particles velocity was retrieved from the particles position at two successive time instants. A statistical analysis has been performed within cubic bins to map the scattered instantaneous velocity information onto a Cartesian grid.

The multi-frame measurements have been successful in revealing the presence of three coherent streamwise vortices. Two co-rotating vortices emanate from the wing tip and the flap side edge, respectively, consistently with the lift discontinuity imposed at these locations. The third streamwise vortex is counter-rotating with respect to the former two and is generated above the engine nacelle due to the interaction between the propeller-induced flow and the external flow on the suction side of the wing. The double-frame measurements at 50 m/s confirm the presence of a strong wing tip vortex that maintains its spatial coherence throughout the extent of the measurement domain. A comparison between the multi-frame and double-frame measurements has been conducted in the wing tip region. It is shown that the double-frame measurements return a lower and broader vorticity peak as a result of the lower spatial resolution and of the higher meandering amplitude of the tip vortex at the higher Reynolds number. Furthermore, it is concluded that the multi-frame measurements are superior to the double-frame measurements in terms of spatial resolution and measurement accuracy.

Future works will focus on enhancing the accuracy of the RVV system for flow measurements at U_∞ = 50 m/s and above to enable applications of the technique for aerodynamic research and development in aeronautics. Possible improvements include: integration of the HFSB seeding rake in the settling chamber of the wind tunnel, so to achieve higher concentration of tracer particles; use of cameras with

higher acquisition frequency (of the order of a few kilohertz) to enable multi-frame measurements at higher flow speed; advanced approaches for the statistical analysis from scattered velocity data to enhance the measurement spatial resolution [19].

5 References

[1] Castaño Sanchez AN, Rodriguez Cisneros E, Angel Blasco EJ. C-295 AEW aerodynamic design process: CFD, wind tunnel tests and flight tests. *Fluid Dynamics and Co-located Conferences*, San Diego, CA, 2013.

[2] Pengel K, Kooi JW, Raffel M, Willert C and Kompenhans J. Application of PIV in the large low speed facility of DNW, *In New Results in Numerical and Experimental Fluid Mechanics* (pp. 253-258). Vieweg+ Teubner Verlag, Wiesbaden, 1997.

[3] Roosenboom EWM, Heider A and Schröder A. Investigation of the propeller slipstream with particle image velocimetry, *J Aircraft*, 46(2), 2007.

[4] Kompenhans J, Dieterle L, Raffel M, Monnier JC, Gilliot A, De Gregorio F and Pengel K. Particle Image Velocimetry: status of development and examples of application in industrial test facilities, *Proc. 3rd ONERA-DLR Aerospace Symposium*, Paris, France, June 20-22, 2001.

[5] Arnott AD, Schneider G, Neitzke KP et al. Detailed Characterisation, using PIV, of the Flow around an Airfoil in High-Lift Configuration. *In: Stanislas M, Westerweel J, Kompenhans J (eds) Particle Image Velocimetry: Recent Improvements.* Springer, Berlin, Heidelberg, 2004.

[6] Veldhuis LLM, Scarano F and Wijk C. Vortex wake investigation of an Airbus A340 model using PIV in a towing tank. *21st AIAA Applied Aerodynamics Conference*, 3814, Orlando, FL (US), 2003.

[7] Sinnige T, Ragni D, Eitelberg G and Veldhuis LLM. Mitigation of pusher-propeller installation effects by pylon trailing-edge blowing. *J Aircraft*, 54(1), 2017.

[8] Bosbach J, Kühn M and Wagner C. Large scale particle image velocimetry with helium filled soap bubbles. *Exp Fluids*, 46: 539-547, 2009.

[9] Scarano F, Ghaemi S, Caridi GCA, Bosbach J, Dierksheide U and Sciacchitano A. On the use of helium-filled soap bubbles for large-scale tomographic PIV in wind tunnel experiments. *Exp Fluids* 56(2): 42, 2015.

[10] Caridi GCA, Ragni D, Sciacchitano A and Scarano F. HFSB-seeding for large-scale tomographic PIV in wind tunnels. *Exp Fluids*, 57(12), 190, 2016.

[11] Caridi GCA, Sciacchitano A and Scarano F. Helium-filled soap bubbles for vortex core velocimetry. *Exp Fluids*, 58(9), 130, 2017.

[12] Schneiders JFG, Jux C, Sciacchitano A and Scarano F (2018). Coaxial volumetric velocimetry. *Meas Sci Technol*, 29(6), 2018.

[13] Jux C, Schneiders JFG, Sciacchitano A and Scarano F (2018). Robotic volumetric PIV of a full-scale cyclist. *Exp Fluids*, 59:74, 2018.

[14] Schanz D, Gesemann S and Schröder A. Shake-The-Box: Lagrangian particle tracking at high particle image densities. *Exp Fluids*, 57(5):70, 2016.

[15] Sciacchitano A and Scarano F. Elimination of PIV light reflections via a temporal high pass filter. *Meas Sci Technol*, 25(8): 084009, 2014.

[16] Wieneke B. Iterative reconstruction of volumetric particle distribution. *Meas Sci Technol*, 24(2): 024008, 2012.

[17] Lynch KP and Scarano F. A high-order time-accurate interrogation method for time-resolved PIV. *Meas Sci Technol*, 24: 035305, 2013.

[18] Beresh SJ, Henfling JF and Spillers RW. Meander of a fin trailing vortex and the origin of its turbulence. *Exp fluids*, 49(3):599-611, 2010.

[19] Agüera N, Cafiero G, Astarita T and Discetti S. Ensemble 3D PTV for high resolution turbulent statistics. *Meas Sci Technol*, 27: 124011, 2016.

Copyright Statement